A Numerical Study of Global Bifurcations in Chemical Dynamics

Global bifurcations are frequently encountered in the dynamic behavior of chemically reacting systems and their models. They cause dramatic qualitative changes in the system response, such as the birth and death of oscillations and even the onset of chaos. They involve entire regions of the system phase space, and due to their nature they are in general not predictable by standard local bifurcation methods, analytical or numerical. Special methods and algorithms must therefore be developed to locate and analyze them in parameter space. This paper presents such methods and algorithms and illustrates them through standard chemical engineering examples. Test cases include lumped chemical reactor models (homogeneous and heterogeneous, autonomous and periodically forced), a problem of compressible gas flow in porous media, and a case of two coupled oscillators. The phenomena discussed include infinite-period bifurcations, saddle connections, frequency locking, and the creation and extinction of multifrequency responses through global manifold interactions (homoclinic tangles).

I. G. Kevrekidis
Center for Nonlinear Studies
and Theoretical Division
Los Alamos National Laboratory
Los Alamos, NM 87545

Overview

Chemically reacting systems and their models are known to exhibit a fascinating variety in their dynamic behavior, including multiple steady states and several types of periodic and aperiodic oscillations (Pismen, 1980). Such phenomena are caused by their inherent nonlinearities, the most common of which is the Arrhenius temperature dependence of the reaction rate. Any systematic effort to understand, analyze, and potentially exploit this behavior involves a detailed numerical or experimental search in operating parameter space, trying to locate critical parameter values for which a dramatic change (a bifurcation) occurs in the system dynamics. If this search is performed experimentally, or through simple computer simulation (i.e., by solving the initial-value problem), only stable, attracting states will be observed. Such states are stable to infinitesimal perturbations (locally stable), but it is quite possible that finite perturbations—whether computational or experimental—may destabilize them, and the system will eventually end up at some other state. A typical example is a continuous stirred-tank reactor (CSTR) in the regime where three steady states, two of them stable, coexist (Uppal et al., 1974, 1976). Unless a large number of initial conditions are tried for the same values of the operating parameters, one can never be absolutely sure of the global picture, that is, of all possible fates of all possible trajectories for the system.

If numerical methods of bifurcation theory are used, including continuation of solutions in parameter space and the computational location of both stable and unstable trajectories, the linearization around the located solution usually yields a quantitative description of its local stability (Iooss and Joseph, 1980; Guckenheimer and Holmes, 1983). A number of general-purpose bifurcation codes have become available during the last decade and have been successfully applied to models of reacting systems. Examples are AUTO (Doedel, 1981), DERPAR (Kubicek and Marek, 1983) and BIFOR2 (Hassard et al., 1981). In a one-parameter search such codes detect critical values for which a solution branch loses stability; they search for and switch on the new, bifurcating branch of solutions that usually is born there. The existence of multiple attractors may thus be predicted systematically, especially in multiparameter searches and through methods such as singularity theory (Balakotaiah and Luss, 1982; Pismen, 1986; Golubitsky and Schaeffer, 1985; Farr and Aris, 1986). These local bifurcations are signalled by a change in the nature of the linearization of the system equations close to the located solution or, in the case where the linearization fails, of higher derivatives again close to this solution.

We are concerned in this paper with a number of transitions

The present address of the author is Department of Chemical Engineering, Princeton University, Princeton, NJ 08544.

in the dynamic behavior of reacting systems—and more generally, dynamical systems—capable of causing dramatic changes in the observable system behavior but intractable by traditional local bifurcation methods and algorithms. It is well known that when two stable steady states coexist for a CSTR, a third, saddle-type steady state also exists, and it lies on a separatrix, that is, a special set of initial conditions that constitute the boundary of the basins of attraction of the two stable steady states: they separate the initial conditions that eventually end up on one stable state from those that will be attracted to the other. It is interesting that global bifurcations often involve precisely such separatrices. Since they occur over entire regions of phase space and not just in the neighborhood of a single solution, they cannot be revealed by the linearization or a few derivatives of the system equations around that solution. While some of the concepts involved, along with certain implications for the system dynamics, may sometimes appear esoteric to the nonmathematician, the phenomena are by no means rare or difficult to observe in the dynamics of chemically reacting systems.

Our main task is to present a number of computational methods and algorithms for the accurate location of a number of global bifurcations in the parameter space of nonlinear systems. Our examples have been chosen so as to point out that such phenomena are ubiquitous even at the simplest modeling level of reactor dynamics. Test cases include infinite-period bifurcations for a homogeneous autocatalytic as well as a heterogeneous catalytic lumped reactor, a heteroclinic saddle connection for a problem of compressible gas flow in porous media, and a case of two coupled oscillators. All these models involve two coupled nonlinear ordinary differential equations (ODE's). We also examine certain global bifurcations that occur in higher dimensional systems; more specifically, we study the creation and extinction of multifrequency oscillations through frequency locking and global manifold interactions. We use a periodically forced autocatalytic reaction (a Brusselator) to illustrate these phenomena, and we present some interesting features of the structure of resonances and representative pictures of homoclinic tangles. We discuss the apparent similarities and differences of these phenomena with the corresponding phenomena in two-dimensional systems. We also discuss some interesting interactions between computational and experimental work and we conclude with some comments on the direction of computational research on global dynamical phenomena.

I: Systems with Two Degrees of Freedom

Introduction

Every chemical engineer has observed the sudden death of limit cycle branches in the now classical analysis of the dynamics of the CSTR by Uppal et al. (1974, 1976). This phenomenon is different from both a typical Hopf bifurcation and a turning point on a branch of limit cycles where two oscillations, one stable and one unstable, collide and disappear (Iooss and Joseph, 1980). It is a particular case of the so called infinite-period bifurcation. A saddle-type unstable steady state essentially collides with the limit cycle, and that marks the end of the limit cycle branch.

This is probably the simplest occurrence of homoclinicity, and it has been known since the 19th century. Bendixson (1901) and Dulac (1923) analyzed it, and the work of Andronov and Leontovic (1971) on this subject for two-dimensional systems is definitive. Even though such bifurcations involve a saddle-type steady state, they cannot be detected through the local information (e.g., linearization) around this steady state. Local information constitutes the foundation of the analytical and numerical bifurcation analysis of systems of ordinary differential equations (location, continuation, and stability determination for steady state branches, direction and stability of limit cycle branches, etc.) as seen for example in Guckenheimer and Holmes (1983) or Iooss and Joseph (1980).

This part of the paper addresses precisely the need for algorithms designed to locate such global phenomena. Two distinct algorithms for two-dimensional systems are presented. The first is a natural extension of a recent algorithm for the computation of invariant circles of maps (Kevrekidis et al., 1985) and is used to study the death of a limit cycle branch of the Gray-Scott autocatalytic model. The second algorithm is our implementation of a procedure described by Hassard (1980) and is applied to a surface reaction model. We discuss the similarities and differences of the two algorithms, and show how to modify them so as to compute heteroclinic saddle connections. We illustrate this modification through a nonlinear eigenvalue problem resulting from compressible gas flow in a porous medium. We then discuss briefly the annihilation of a limit cycle by the appearance of a saddle node (a marginally stable steady state) on it. This case is remarkably similar to frequency locking on a torus. We describe such higher dimensional phenomena in part II, below.

Invariant Curve Method

Gray-Scott scenario

In recent papers Gray and Scott (1983, 1984) have studied the dynamics of the autocatalytic reactions $A \rightarrow B$ with rate proportional to $[A][B]^n$ in an isothermal CSTR. We are interested in the cubic irreversible autocatalysis scheme

$$A + 2B \rightarrow 3B, \quad B \rightarrow C \tag{1}$$

for which the open CSTR rate equations become

$$\begin{aligned} dx/dt &= -k\,x\,y^2 + \theta\,(1 - x) \\ dy/dt &= k\,x\,y^2 + \theta\,(y_0 - y) - y \end{aligned} \tag{2}$$

where x and y are the dimensionless concentrations of species A and B, respectively, k is the reaction rate, and $\theta = 1/\tau$, the inverse of the residence time. We examine a feature of the bifurcation diagram obtained for $y_0 = 1/15$ and $k = 40$ as θ varies. At $\theta = 0.3$ the system of Eqs. 2 has a unique stable focus in its phase plane, Figure 1a. At $\theta = 0.19568172$ this steady state undergoes a Hopf bifurcation, loses stability, and gives birth to a stable (attracting) limit cycle, Figure 1b. The limit cycle grows as we decrease θ, and every trajectory on the phase plane—except for the one starting precisely at the unstable steady state—becomes eventually attracted to the limit cycle. The stability of this oscillation is quantified by its characteristic (Floquet) multipliers, one of which remains pinned at 1 while the other, being also 1 at the Hopf bifurcation, becomes less than 1 as we decrease θ. At $\theta = 0.12876385$ a qualitative change occurs on the phase plane: a saddle-node (turning point) bifurcation occurs in the interior of the limit cycle, and two new steady states, a stable node and a saddle, come into play. They move apart as θ decreases further. The situation is illustrated in Figures 1c and 1c′ for $\theta =$

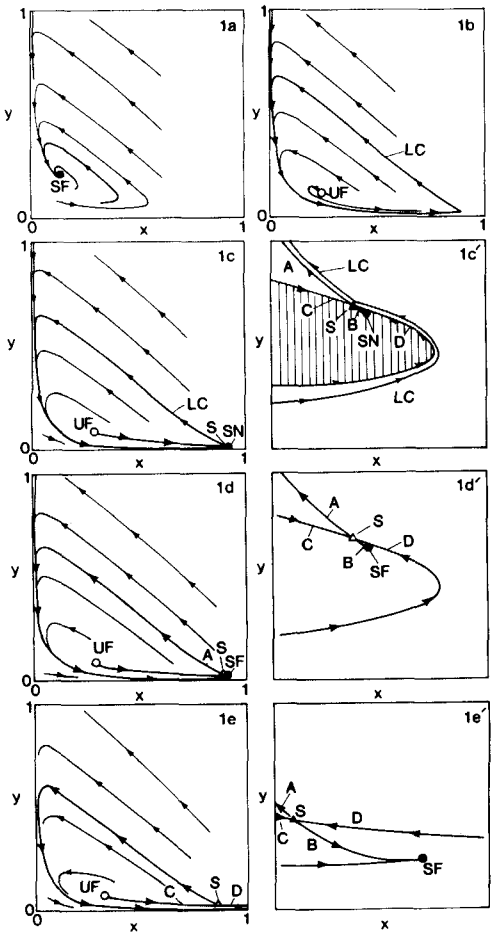

Figure 1. Phase plane details of an infinite period bifurcation of the Gray-Scott "autocatalator."

0.128751. Three steady states exist: a stable node *SN*, a saddle *S*, and an unstable focus *UF*. All three are surrounded by a stable limit cycle *LC*. Two attractors, the stable node and the stable limit cycle, coexist, and we locate the basins of attraction for each of them (i.e., the sets of initial conditions that are attracted to each one). Observe the line segments *SA, SB, SC*, and *SD* that emanate from the saddle *S*. *SC* and *SD* consist of points (x, y) such that $\phi_t(x, y) \rightarrow S$ as $t \rightarrow \infty$, where $\phi_t(x, y)$ is the result of integrating the system of Eqs. 2 with initial conditions (x, y) for time duration t. The set of all such points $W^s(S)$ is the stable manifold of the saddle point *S*. On the other hand, *SA* and *SB* consist of points (x, y) such that $\phi_t(x, y) \rightarrow S$ as $t \rightarrow -\infty$. The set of all such points is the unstable manifold $W^u(S)$ of the saddle *S*. By the stable manifold theorem for a fixed point (Hirsch et al., 1977), at the saddle *S* each manifold is tangent to an eigenvector of the linearization of the system of Eqs. 2—the Jacobian matrix—at *S*. The stable manifold is tangent to the eigenvector corresponding to the eigenvalue $\lambda_1 < 0$, and the unstable manifold to that corresponding to $\lambda_2 > 0$. These are standard definitions, making our discussion more concise. For more details on the definitions and the theorems see Guckenheimer and Holmes (1983).

Let us now observe the regions of attraction of the limit cycle and the steady state: *SC* and *SD* are both coming near each other and spiral toward the unstable focus *UF*. Every point in the shaded region they define, Figure 1c', is attracted to the stable node *SN*. Everything outside that region gets attracted by the limit cycle *LC*. The two branches of the stable manifold $W^s(S)$ form a separatrix between the basins of attraction of the two attractors. The two parts of the unstable manifold eventually become attracted, *SA* by the limit cycle and *SB* by the stable steady state.

As we further decrease θ, the limit cycle develops a "dent" close to the saddle *S*. It comes closer and closer to the parts *SA* of the unstable manifold and *SD* of the stable manifold. (Meanwhile, *SN* has changed to a stable focus *SF*—λ_1, λ_2 complex with negative real part—but it is still attracting, and this does not affect the phenomenon we are interested in.) The period of the limit cycle becomes larger, and the phase point spends the largest part of this period in the neighborhood of the saddle. This is quantified by the second, free, Floquet multiplier, which approaches zero.

At $\theta = \theta_h = 0.12874791$ a qualitative change occurs. The limit cycle ceases to exist. It is replaced by a closed loop that consists of one part (*SA*) of the unstable manifold, that now coincides with one part (*SD*) of the stable manifold. The saddle *S* also lies on this loop. It takes infinite time for a point on *SA* to reach *S* through *SD*. We thus say that the limit cycle undergoes an infinite-period bifurcation, Figures 1d and 1d'. This situation is structurally unstable, meaning that it occurs for only one specific value in our one-parameter study. For $\theta > \theta_h$ we have a limit cycle and a stable steady state, each with its own region of attraction. For $\theta < \theta_h$ we only have a stable steady state. The whole phase plane (except *UF, SC*, and *SD*) gets attracted to it. At $\theta = \theta_h$ we say that we have a homoclinic loop because the stable and unstable manifolds of the same saddle coincide.

For $\theta < \theta_h$ both parts *SA* and *SB* are attracted by the stable steady state. Comparing Figures 1c' and 1e' we see that *SD* was "inside" *SA* before the homoclinic loop ($\theta > \theta_h$), and now is "outside" it. Figure 1e ($\theta = 0.12$) shows that a closed loop still exists in the phase plane. It consists of the two parts of the stable manifold *SA* and *SB*, and the stable focus *SF*. This loop may not be smooth (there is an infinite spiral at *SF*, and when *SF* becomes a stable node at $\theta = 0.09097622$ there will be a cusp there) but its existence is nevertheless crucial to our first algorithm.

Both before and after the homoclinic loop, a closed loop exists in the phase plane: for $\theta > \theta_h$ it is the limit cycle; after the homoclinic loop ($\theta < \theta_h$) it is the combination *SA(SF)SB*. Both are closed loops and both are invariant under the system equations (every trajectory that starts on them stays on them for all positive time). Their fundamental difference is that the limit cycle is a trajectory of the system of ODE's, Eqs. 2, but the loop *SA(SF)BS* is not a trajectory. The limit cycle can be solved for (along with its period) through shooting or polynomial approximation methods for boundary value problems (BVP's) (Doedel, 1981; Seydel, 1981). The loop *SA(SF)BS* however cannot be solved in principle as a BVP.

It is possible to formulate a procedure, illustrated in Figures 2a and 2b, that will conceptually converge to both types of closed loops. Suppose that only a stable limit cycle *LC* exists in the phase plane. We consider an infinity of initial conditions that lie on a closed loop $S^{(1)}$ that surrounds *LC*. The result of integrating the system equations, starting from every point on $S^{(1)}$ for some time t (the same for all initial conditions)—that is, constructing the time t return map for each point on $S^{(1)}$—will

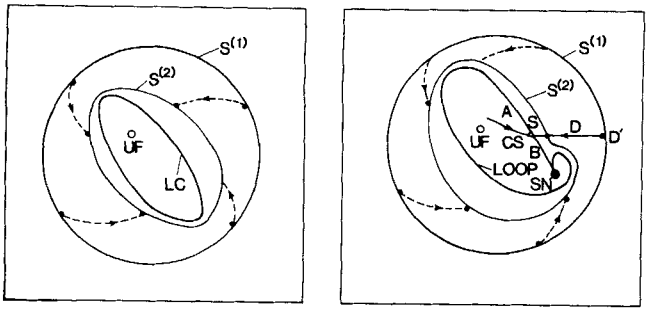

Figure 2. Schematic tracking of a one-parameter family of initial conditions: before (left side) and after (right-side) occurrence of a homoclinic loop.

be another closed curve $S^{(2)}$ surrounding LC but closer to it. Repeating this procedure again and again, $S^{(n)} \rightarrow LC$ as $n \rightarrow \infty$. Instead of simply iterating, we can construct a contraction mapping (e.g., a Newton-Raphson iterative procedure) to converge on LC as the circle S—whose image $S^{(1)}$, obtained by taking each point on the circle and integrating for time t—coincides with itself. We have performed such computations for maps (Kevrekidis et al., 1985), and an example of such a computation is shown in Figure 3a. It is probably clumsy, or at best equivalent to a multiple shooting method (Schwartz, 1983), to compute a limit cycle this way. Indeed, the power of the procedure lies in the case of Figure 2b when we are beyond the homoclinic loop, and the limit cycle does not exist any more. The only existing loop is the one formed by the unstable manifold of the saddle SA and SB and the stable steady state SN. Consider again an infinity of initial conditions lying on the closed loop $S^{(1)}$. By constructing the time t return map for each of these conditions for some t, we obtain another closed loop $S^{(2)}$. Proceeding in the same way to $S^{(3)}$, $S^{(4)}$, etc., we finally converge to the loop $SA(SN)BS$. The whole concept lies in iterating the entire $S^{(i)}$ as a curve. If each point on $S^{(1)}$ were left to run forward in time individually, all except D' that lies on SD would collapse to SN. Iterating the closed curve as an entity converges to the loop. As an alternative to this simple iteration, we have constructed an algorithm that converges to $SA(SN)BS$ quadratically. There exist of course issues of discretization and parameterization of the curve, especially due to the cusp at SN (or the infinite spiral if we have a focus SF), but these can be considered at this stage as technical details. The main idea is to consider the fate not of separate initial conditions, but of whole sets of them that have some common property (in this case they lie initially on a closed one-parameter curve).

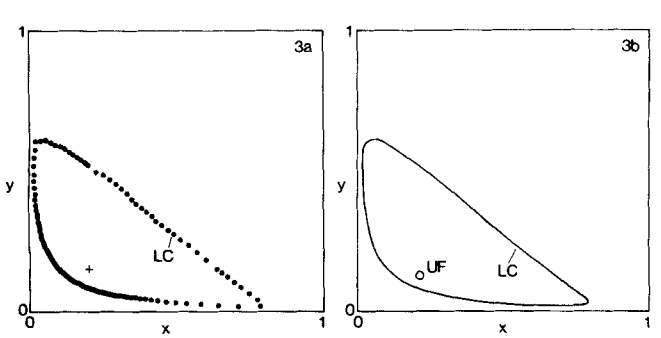

Figure 3. Limit cycle of the Gray-Scott model.
(a) Obtained as an invariant circle of time t map
(b) Obtained as solution of a shooting algorithm

Description of the algorithm

In order to locate the homoclinic loop, we must compute the loop itself along with the parameter value θ_h for which it occurs. We are essentially looking for an invariant closed curve (invariant under the time t return map for some t). Such curves exist both before and after θ_h. We have previously described (Kevrekidis et al., 1985) an algorithm for finding them: We discretize say N points, create the images of the N points, interpolate between the image points to obtain the image curve, and finally take the difference between archetype and image curve at the N discretization points. This procedure results in N nonlinear coupled algebraic equations with N unknowns.

In order to locate one special loop, the homoclinic loop, we must append one extra equation to be solved along with these N equations. This equation will be used to find the parameter value θ_h for which the homoclinic loop occurs. At first sight it may appear that the special characteristic of the homoclinic loop from which this extra equation stems is that the saddle S should lie on the loop. Figure 2b however shows that this happens for all $\theta < \theta_h$. At the homoclinic point, and only there, the saddle connection contains a part of the stable manifold of the saddle point. This dictates that the $N + 1$ equation must express the condition:

A point on the stable manifold of the saddle should lie on the loop at the homoclinic saddle connection.

Approximations to the stable (or unstable, for that matter) manifolds in the neighborhood of the saddle S can easily be constructed. The construction is based on first and higher order derivatives at the saddle point, and Hassard (1980) gives estimates of the error bounds as higher order terms are used. The simplest construction is to compute the eigenvectors at the saddle point and use some point on them. (This is a first-order approximation to the manifolds, based on the stable manifold theorem.) If we adopt this construction for simplicity, our procedure should be as follows:

1. Guess a discretization $\underline{x}_i^{(1)}$ ($i = 1, 2, \ldots, N$, $\underline{x}_1 = \underline{x}_{N+1}$) of the loop, and a parameter value $\theta^{(1)}$.

2. Find (through an intermediate Newton-Raphson procedure) the saddle point $S(\theta^{(1)})$. Construct a point $\underline{X}_{SM}(\theta^{(1)})$ that lies on the stable manifold of $S(\theta^{(1)})$.

3. Obtain the images of the time t return map for the points $\underline{x}_i$ by integrating the system equations with initial conditions $\underline{x}_i$ for time t. Interpolate between them to get the image curve $\underline{y}_i$.

4. Take the N distances $\underline{x}_i - \underline{y}_i$ as well as the distance $\underline{X}_{SM}(\theta^{(1)}) - \underline{Y}$, where $\underline{Y}$ is the point on the image curve corresponding to $\underline{X}_{SM}$ in the particular parameterization we are using.

5. Require that these $N + 1$ distances be zero. This gives $N + 1$ equations with $N + 1$ unknowns. Derivatives in the Jacobian of the Newton method for this set of equations require integration of variational (for the $\partial \underline{y}_i / \partial \underline{x}_j$) and sensitivity (for the $\partial \underline{y}_i / \partial \theta^{(1)}$) equations along with the construction of the return map. The derivatives of the last equation (the $N + 1$ equation for $\underline{X}_{SM}$) can be partly computed through higher order local derivatives at the saddle point.

We applied full Newton iteration in our implementation of this algorithm. The convergence was quadratic, and the results

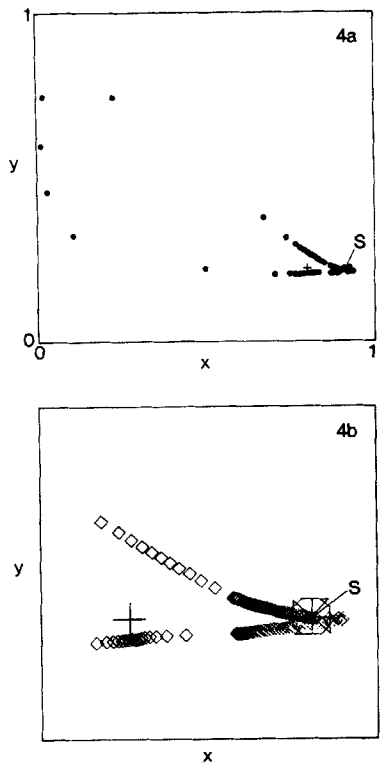

Figure 4. Results of the invariant circle algorithm.
(a) Converged homoclinic loop
(b) Enlargement of lower righthand corner of (a)
●◇ mesh points; ◌ point on stable manifold of saddle
✠ saddle; + centerpoint of polar parametrization

are shown in Figures 4a and 4b. The saddle point and the point on the stable manifold are also shown. We do not concern ourselves here with numerical analysis aspects of the algorithm; we will return to them on another occasion. Suffice it to say that for this problem, we found it to be remarkably robust to different (and sometimes poor) discretizations around the saddle point.

Trajectory Method

Problem statement

The algorithm in the previous section was based on locating an invariant object (a loop), not on locating a trajectory of the system of ODE's. It is however possible to formulate the saddle connection problem so as to end up looking for a trajectory, by separating it in three stages (Hassard, 1980). It takes infinite time for a point A on the unstable manifold SA to reach S backward in time, Figures 1d and 1d'; it also takes infinite time for a point D on the stable manifold SD to reach the saddle forward in time. However, it takes a finite time for the phase point to travel from a given point A on SA to a given point D on SD. The procedure should now be obvious: since we can approximate the stable and unstable manifolds in a neighborhood of the saddle, we can construct points A and D on them, respectively. This removes the "infinite time" singularity at S, and now we can solve with traditional methods for the trajectory AD. Due to the finite time between A and D, this is a simple boundary value problem. We now describe our implementation for a heterogeneous catalytic CSTR.

Surface reaction scenario

Investigating the simplest reaction rate nonlinearities that might lead to oscillatory behavior in surface catalytic reactions, Takoudis et al. (1981) proposed the following mechanism (where S is a catalytic site):

$$\begin{aligned} &A_{gas} + S \rightarrow AS \text{ (adsorbed)} \\ &B_{gas} + S \rightarrow BS \text{ (adsorbed)} \\ &\frac{AS + BS + 2S \rightarrow C\uparrow + 4S}{A + B \rightarrow C \text{ (overall reaction)}} \end{aligned} \tag{3}$$

Gaseous reactants A and B flow in a heterogeneous CSTR. They adsorb and desorb competitively with Langmuir-Hinshelwood kinetics, but they also react to product C, which for simplicity is taken to desorb immediately. The reaction mechanism requires two vacant sites, and if the conversion is small, so as to consider it differential, or if the gas phase pressures of reactants A and B are maintained constant, the equations of change become

$$\begin{aligned} d\theta_A/dt &= \alpha_1(1 - \theta_A - \theta_B) - \gamma_1\theta_A - \theta_A\theta_B(1 - \theta_A - \theta_B)^2 \\ d\theta_B/dt &= \alpha_2(1 - \theta_A - \theta_B) - \gamma_2\theta_B - \theta_A\theta_B(1 - \theta_A - \theta_B)^2 \end{aligned} \tag{4}$$

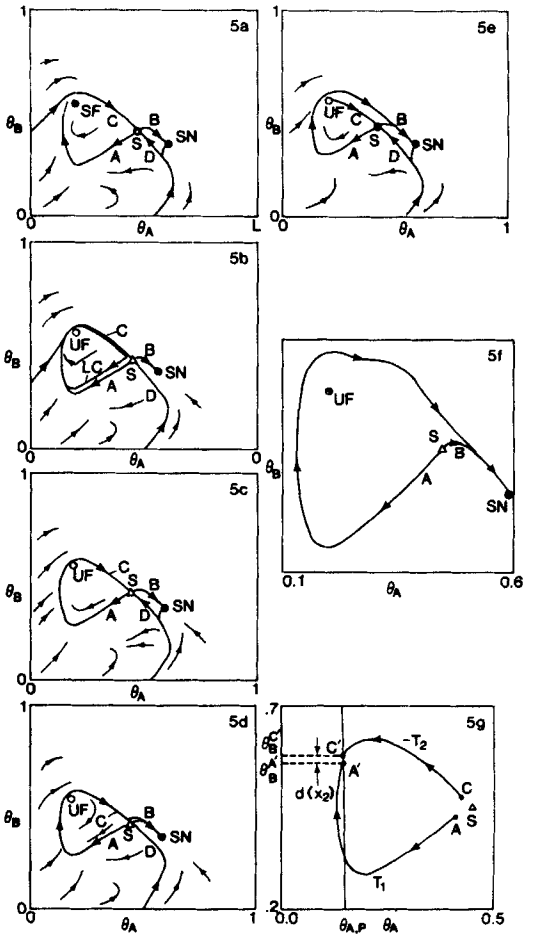

Figure 5. (a)–(f) Surface reaction homoclinic loop. (g) Illustration of the double-shooting algorithm.

where θ_A and θ_B are surface coverages (submonolayer) of adsorbed A and B, α_1 and α_2 are dimensionless gas phase pressures of A and B, respectively, and γ_1 and γ_2 are dimensionless desorption rates.

We are concerned with a feature of the bifurcation diagram of the system of Eqs. 4 obtained for $\gamma_1 = 0.001$, $\gamma_2 = 0.002$, and $\alpha_1 = 0.025$ as α_2 is varied. Starting at $\alpha_2 = 0.029$, the system of Eqs. 4 has three steady states: one stable node *SN*, one unstable saddle *S*, and a stable focus *SF*, Figure 5. The two arms *SC* and *SD* of the stable manifold of the saddle *S* create a separatrix between the basins of attraction of the stable steady states *SN* and *SF*. The two arms of the unstable manifold are attracted to these stable states, *SB* to *SN* and *SA* to *SF*. There is a Hopf bifurcation at $\alpha_2 = 0.029469$ and the stable focus loses stability, shedding a stable limit cycle *LC*. The arm *SA* of the unstable manifold now winds toward this limit cycle, while *SN*, *SD*, and *SB* remain practically the same, Figure 5b. As α_2 grows, the limit cycle also grows and approaches the saddle and *SC*. At $\alpha_2 = \alpha_h = 0.029483885486$ a homoclinic loop is observed: *SA* and *SC* coincide, and the limit cycle is lost in an infinite-period bifurcation, Figure 5c. After $\alpha_2 = \alpha_h$, the whole phase plane has only one attractor, the node *SN*. The stable manifold *SN* is now inside the unstable manifold loop *SA(SN)BS*, Figures 5d and 5e, and goes to the unstable focus *UF*. The cusp at *SN* is quite characteristic, and so is the behavior of *SA:* it stays close to *SC* until a certain point, when it gets attracted to the weak attracting eigendirection *(SN)E* of the stable steady state. This is also a nice case to illustrate the global iteration procedure described in the previous section. The results of iterating a whole loop of initial conditions are shown in Figure 5f for $\alpha_2 = 0.0294838$ when we have an unstable manifold loop *SA(SN)BS*. Because of the cusp at *SN*, the loop in Figure 5f was parameterized with percent total arclength.

Description of the algorithm

We have simplified our implementation of this algorithm so that its structure becomes more apparent and so that one thing is solved for at a time.

1. We guess a value $\alpha_2^{(1)}$ for the parameter value $\alpha_{2,h}$ at which the homoclinic loop occurs. For this $\alpha_2^{(1)}$ we locate the saddle point coordinates (θ_A, θ_B) *saddle* at $\alpha_2^{(1)}$.

2. We construct a point C on the stable manifold and a point A on the unstable manifold of the saddle S, Figure 5. Several degrees of approximation in the construction of the manifolds are possible. In the simplest case, we compute the normalized eigenvectors of the Jacobian at the saddle point, and choose points that lie at an arbitrary (but constant throughout the main iteration) distance away from the saddle. We have thus eliminated the "infinite time" parts of the problem.

3. In order to find a trajectory that connects A with C we use a double-shooting algorithm. We choose a Poincare section (say the line $\theta_A = \theta_{A,P}$). We shoot from A forward in time until we reach the point A' for which $\theta_A = \theta_{A,P}$. This requires a Newton iteration (one equation with one unknown) that yields the time T_1 needed to go from A to A'. We also shoot backward in time from C until we reach the point C' for which $\theta_A = \theta_{A,P}$. This is again a Newton iteration that yields one unknown $(-T_2)$.

4. When the distance $\theta_B^{A'} - \theta_B^{C'}$ is zero, we have constructed an approximation to the homoclinic loop. The equation

$$\theta_B^{A'}(\alpha_2) - \theta_B^{C'}(\alpha_2) = 0 \tag{5}$$

is a function of only one unknown, the parameter α_2, and can be solved through a Newton iteration to give finally, after convergence, $\alpha_{2,h}$. It is important to notice that the chain rule will be applied several times in order to obtain the derivatives with respect to α_2 above.

5. The algorithm does indeed converge quadratically to $\alpha_{2,h}$, and due to its segmentation is easier to implement and check than the invariant curve algorithm. The double shooting helps in the case of α_2 trial values for which it is impossible to construct an equation like Eq. 5 with simple shooting.

Heteroclinic Saddle Connections

We so far have described the computation of saddle connections for two-dimensional dissipative systems. Quite often, however, heteroclinic orbits are observed in dynamical systems: the unstable manifold of a saddle steady state coincides with the stable manifold of another (hetero-), not the same (homoclinic) saddle point. Both the rationale and the algorithms described above remain essentially the same in this case. Here is an example of this phenomenon; another example can be found in Pismen (1986).

Nonlinear eigenvalue problem

Let $u = u(x, t)$ represent the appropriately scaled density of an ideal gas flowing isentropically in a homogeneous d-dimensional porous medium. Then, according to classical theory (Muskat, 1937) the evolution of u is governed by the equation

$$\partial u(x, t)/\partial t = \Delta(u^m) \tag{6}$$

where Δ represents the d-dimensional Laplace operator and m is a constant that satisfies $m > 1$. Equation 6 is a nonlinear parabolic equation that is degenerate in a neighborhood of any point where $u = 0$. In the linear diffusion case ($m = 1$) it is well known that there is an infinite speed of propagation of disturbances from rest. Perhaps the most striking manifestation of the nonlinear degeneracy in Eq. 6 is the finiteness of this speed. Thus, if the gas is initially confined to a bounded subregion of an infinite medium, then the part of the medium occupied by gas will remain bounded for all finite times (although it will ultimately expand). In these circumstances, the moving gas front is an object of particular interest.

Consider a radially symmetric flow with the gas initially occupying the exterior of a sphere centered at the origin. As time increases, the gas flows into the sphere and completely fills it at some finite time T. J. Graveleau has proposed a self-similar solution to this problem that has particular theoretical interest. Specifically, we look for a radially symmetric solution of the type $u = u(|x|, t) \in \mathcal{R}^d \times \mathcal{R}^-$ with $u(|x|, 0) = |x|^{2-\alpha}$ (Aronson, 1986) for some $\alpha \in [1, 2)$. Assuming that $u(|x|, t) \equiv -(r^2/t)\,\phi(\eta)$ with $\eta = |x|^{-\alpha}t$, substituting in Eq. 6 with conditions $\phi(0) = 0$, $\phi'(0) = 1$, we obtain a second-order ODE. By further setting $\eta = -e^{-\xi}$ and introducing the variable τ such that $d\tau/d\xi = 1/\psi(\xi)$ we arrive at the system of ODE's

$$\begin{aligned} d\theta/dt &= (\tfrac{1}{2}\alpha^2)\,\psi + (\tfrac{1}{2}\alpha^2)\,\theta - (k/2\alpha^2)\,\psi^2 \\ &\quad - [(b + d)/\alpha]\,\psi\theta - \theta^2 \\ d\psi/dt &= \theta\psi \end{aligned} \tag{7}$$

The problem of finding Graveleau's solution can be reduced

to the problem of finding a heteroclinic orbit for the system of Eqs. 7. This system has three steady states: the saddles (0, 0) and (0, $\frac{1}{2}\alpha^2$), and the point (0, $1/k$). The details of the problem and the derivation are given by Muskat (1937) and Aronson (1986). The purpose of this example is to illustrate the computation of a heteroclinic saddle connection and to show the applicability of the methods so far described in an apparently unrelated problem.

Aronson scenario

Let us consider what happens for $m = 3$ and $d = 2$ as α is varied. Initially—$\alpha = 0.8$, Figure 6a—the nonsaddle steady state is an unstable focus. One arm of the stable manifold of the saddle S (0, 0) coincides with the θ axis and with the arm $S'C'$ of the nontrivial saddle S'. We know from the corresponding boundary condition the direction of the stable manifold SC of the trivial saddle S (it has always slope -1). SC gets attracted to the unstable focus UF backward in time. The unstable manifold $S'A'$ of S' extends to infinity.

As α varies, the unstable focus undergoes a Hopf bifurcation, changing to a stable focus and giving birth to an unstable limit cycle LC, Figure 6b, $\alpha = 1.1$. The behavior of the manifolds $S'A'$ and SC remains the same: SC is now attracted to the unstable limit cycle in negative time. At $\alpha = 1.2557502$ the heteroclinic saddle connection occurs: $S'A'$ coincides with SC, while the limit cycle is replaced by the heteroclinic loop $SS'A'CS$, Figure 6c. The value $\alpha_h = 1.2557502$ is the solution to our nonlinear eigenproblem. For $\alpha > \alpha_h$ the situation changes: $S'A'$ gets attracted by the stable steady state, while SC extends to infinity, Figure 6d.

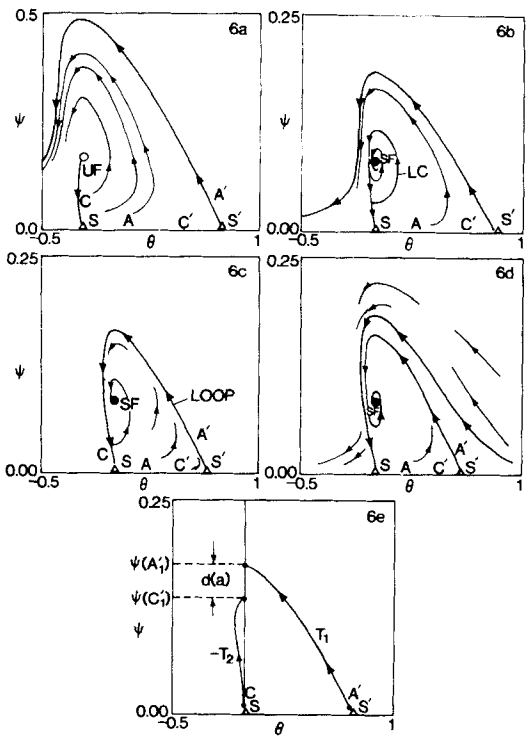

Figure 6. (a)–(d) Heteroclinic loop derived in the context of gas flow in a porous medium.
(e) Illustration of the double-shooting algorithm.

The algorithm described for the trajectory method above is very easily modified to find α_h. We normally should (but need not) iterate for the saddles S and S', which we know explicitly. Hence we can explicitly construct points A', C that lie on the approximate unstable and stable manifolds of S' and S, respectively. We again do a double shooting, forward in time from A' and backward from C. With a simple Newton iteration we find the times that it takes for the trajectories to reach some convenient Poincare section, say $\theta = 0$, Figure 6e. The distance $\psi(A'_1) - \psi(C'_1) \equiv d(\alpha) = 0$ gives us the equation to be solved for α_h. Similar conceptually simple modifications can be applied to our first algorithm: we would solve for an invariant arc starting on $S'(\alpha)$ and ending on C. We tested our algorithms in this case against the analytically obtainable $m = d = \alpha_h = 1$. Even with a simple manifold construction (a point on the eigenvector) we could easily obtain quadratic convergence and an error of 0.4×10^{-9} from the actual homoclinic parameter value.

Andronov-Leontovic Case II

Description

One more possibility of an infinite-period bifurcation (a death of a limit cycle branch) is possible for two-dimensional systems: the appearance of a steady state of the saddle-node type on the limit cycle (sometimes referred to as saddle-node-infinite-period, or SNIPER, bifurcation). Such a sequence is shown schematically in Figure 7. Initially a stable limit cycle surrounds an unstable steady state, Figure 7. Then, as we change some control parameter a saddle node appears on the loop at $\alpha = \alpha_{crit}$, Figure 7b. The saddle node is a marginally stable steady state with one eigenvalue equal to zero and one other than zero. In this case, the loop tends to the saddle node SSN both for $t \to +\infty$ and $t \to -\infty$. As the parameter moves beyond α_{crit} the saddle S and the stable node SN separate, Figure 7c. The integrity of the loop remains intact however. It is again formed by the two arms of

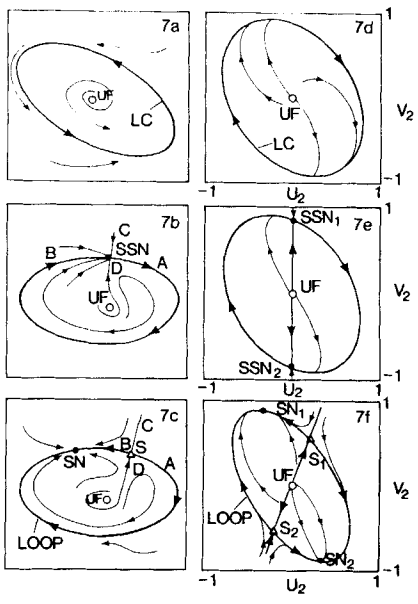

Figure 7. (a)–(c) A saddle-node infinite-period bifurcation.
(d)–(f) Its realization in a problem of coupled oscillators.

the unstable manifold of the saddle SA and SB and the stable node SN. The difference is that SB and SA tend to opposite sides of the weak stable eigendirection of the node SN (the one that corresponds to the absolutely smaller negative eigenvalue), not to the same side as in case I, which was examined in previous sections. The saddle stable manifold does not now separate the basins of attraction of different attractors (hence the term "virtual" as opposed to "actual" separatrix; Abraham and Shaw, 1985).

This sequence is remarkably similar to frequency locking on a torus, a phenomenon we will examine in part II, below. It shares several common characteristics with case I, and the numerical search for it is straightforward. The invariant circle algorithm needs no modification for this case. It easily converges on the closed loop, either before α_{crit} (on the limit cycle) or after α_{crit} [when it finds the "object" $SA(SN)BS$]. The difficulty due to the globality of the bifurcation is essentially nonexistent in this case: the saddle node can be computed and analyzed as a local phenomenon. If we know that our model has generically this type of behavior, we find the parameter value α_{crit} from the turning point saddle-node bifurcation, independently from the entire loop. A very interesting system in which this sequence occurs is the case of two linearly coupled oscillators.

Coupled oscillators

The dynamics of coupled oscillators are important in several fields of science and engineering. Aronson et al. (1987) and Othmer et al. (1986) studied the model problem of two linearly coupled oscillators described by

$$\begin{aligned}
dx_1/dt &= a\,x_1 + b\,y_1 - x_1(x_1^2 + y_1^2) + \delta(x_2 - x_1) \\
&\quad + \delta(y_2 - y_1) \\
dy_1/dt &= -b\,x_1 + a\,y_1 - y_1(x_1^2 + y_1^2) + \delta(x_2 - x_1) \\
&\quad + \delta(y_2 - y_1) \\
dx_2/dt &= a\,x_2 + b\,y_2 - x_2(x_2^2 + y_2^2) + \delta(x_1 - x_2) \\
&\quad + \delta(y_1 - y_2) \\
dy_2/dt &= -b\,x_2 + a\,y_2 - y_2(x_2^2 + y_2^2) + \delta(x_1 - x_2) \\
&\quad + \delta(y_1 - y_2) \qquad (8)
\end{aligned}$$

If we make the change of coordinates

$$\begin{aligned}
u_1 &= (x_1 + x_2)/2, \qquad v_1 = (y_1 + y_2)/2 \\
u_2 &= (x_1 - x_2)/2, \qquad v_2 = (y_1 - y_2)/2 \qquad (9)
\end{aligned}$$

we find that when $u_1 = v_1 = 0$ we have

$$\begin{aligned}
u_2 &= (a - 2\delta)\,u_2 + (b - 2\delta)\,v_2 - u_2(u_2^2 + v_2^2) \\
v_2 &= -(b + 2\delta)\,u_2 + (a - 2\delta)\,v_2 - v_2(u_2^2 + v_2^2) \qquad (10)
\end{aligned}$$

Suppose that $a = 1$ and $b = 0.3$. For $0 < \delta < 0.15$ the system of Eqs. 10 has a stable limit cycle surrounding an unstable steady state, Figure 7d. At $\delta = 0.15$ two saddle nodes appear on the closed loop, Figure 7e. The loop now consists of two steady states and two heteroclinic orbits connecting them. For $0.15 < \delta < 0.2725$ the saddles and the nodes move apart, but the integrity of the closed loop is conserved. It now consists of four steady states and the heteroclinic orbits connecting them, Figure 7f. This loop, as well as the steady states on it, happen to be obtainable in closed form for this problem.

II. Generation of Multifrequency Oscillations

Introduction

The phenomena described in part I above are particular to systems with two degrees of freedom, due to the fact that trajectories of ordinary differential equations do not cross each other (Arnol'd, 1973). New possibilities of interesting behavior arise as more equations and more dimensions become necessary in order to describe the dynamics of a given system. On the other hand, the difficulty of visualizing trajectories and trends in higher dimensional systems becomes increasingly prohibitive. In this part we study some aspects of the dynamics of higher (at least three-) dimensional systems that involve global bifurcations. For simplicity in the computations we will not consider an autonomous system with three coupled equations of change (like the CSTR with two consecutive reactions; Jorgensen et al., 1984); we will instead consider a two-dimensional system (two nonlinear coupled equations) with periodic forcing, which has effectively the same number of variables as the three-dimensional autonomous case.

A convenient way of producing two-dimensional plots of trajectories that lie in a three-dimensional space is to project them on the $x - y$, $y - z$, or $x - z$ planes. An alternative method, which has been extensively used as a tool in the theory of dynamical systems, is to use Poincaré sections. These are obtained by means of choosing some two-dimensional surface Π that intersects (transversally) the system trajectories and, instead of recording a trajectory continuously in time, by recording the sequence of points obtained every time this trajectory crosses the surface Π. By associating each such intersection point with the next one in the sequence we create a map of the surface Π to itself, the Poincaré map associated with Π. Naturally, the "time of flight" of the trajectory between successive intersections varies. For a periodically forced system however, there exists a natural choice for Π, given by

$$\text{Phase } \phi = \omega t \bmod 2\pi \text{ of the forcing term} = \text{constant} \qquad (11)$$

for which the time between consecutive intersections is constant, known *a priori*, and equal to the period of the forcing T. This special case of a Poincaré map is called the stroboscopic map. Entrained periodic trajectories having the same period as the forcing (called period 1 solutions) appear stroboscopically as fixed points of this map. Periodic trajectories whose period is n times the period of the forcing (period n solutions) appear as n distinct (periodic) points of the map. Finally, quasiperiodic trajectories characterized by two frequencies whose ratio is not a rational number (incommensurate frequencies), appear stroboscopically as closed curves (called invariant circles) of the map. Instead of changes being effected continuously forward or backward in time, we observe discrete jumps of the phase point effected by iterating the stroboscopic map (Kai and Tomita, 1979; Kevrekidis et al., 1984, 1986a; Tomita, 1982).

The stability of a periodic solution of the system of equations (a fixed or periodic point of the map) is determined by the linearization of the map around this fixed point. The eigenvalues of this linearization are, in effect, the characteristic (Floquet)

multipliers of the limit cycle on which the point lies (Iooss and Joseph, 1980). The oscillation is stable if these eigenvalues lie within the unit circle in the complex plane, that is, if they have absolute values smaller than unity. A saddle point of the map (lying on a saddle-type oscillatory trajectory) will be characterized by two eigenvalues, λ_1 ($|\lambda_1| < 1$) and λ_2 ($|\lambda_2| > 1$). Global bifurcations in such systems involve interaction of the invariant manifolds (Hirsch et al., 1977; Guckenheimer and Holmes, 1983 of the saddle-type points Σ. These invariant stable and unstable manifolds, $W^s(\Sigma)$ and $W^u(\Sigma)$, respectively, are defined for saddle-type oscillations or fixed points in a conceptually similar fashion with the manifolds of saddle-type steady states in part I. A significant difference is that now these manifolds are surfaces in three-dimensional space, consisting of families of trajectories. When we look at the system stroboscopically on the plane Π: $\{x, y, z = \text{const}\}$ the oscillation reduces to the saddle point Σ, the intersection of the limit cycle with Π. The stable and unstable manifolds of the oscillation will intersect the plane Π along curves. These curves are then the corresponding stable and unstable manifolds of the saddle fixed point of the stroboscopic map. Restricting our observation on the plane Π, we obtain the eigenvectors of the linearization of the stroboscopic map around the fixed point Σ. Then, according to the stable and unstable manifold theorems for maps (Guckenheimer and Holmes, 1983; Hirsch et al., 1977) the curves W^s and W^u in the vicinity of Σ will be tangent to the eigenvectors corresponding to λ_1 ($|\lambda_1| < 1$) and λ_2 ($|\lambda_2| > 1$), respectively.

There exists a crucial difference between the dynamics of this map *of* the plane (and the underlying three-dimensional system) and the dynamics of a two-dimensional system *on* the plane. In a two-dimensional system (Andronov et al., 1971) an entire arm of the unstable manifold of a saddle-type state is in essence one trajectory. Knowing one point on it will give us all other points on it by integrating forward and backward in time. For the stroboscopic map, the same branch of the manifold of the saddle point Σ consists of an infinity (a one-parameter family) of trajectories. The method of averaging (Krylov and Bogoliubov, 1947), a very powerful tool in both theoretical and applied analysis of such systems, tries to simulate the dynamics of the map by a set of ODE's on Π (Greenspan and Holmes, 1984).

Our example throughout this part of the paper will be a forced Brusselator, a homogeneous autocatalytic scheme

$$\begin{aligned} dx/dt &= A + x^2y - Bx - x + \alpha \cos(\omega t) \\ dy/dt &= Bx - x^2y \end{aligned} \tag{12}$$

At zero forcing amplitude ($\alpha = 0$) the autonomous system has a stable limit cycle with frequency ω_0 ($A = 0.4$, $B = 1.2$). Tomita and coworkers (Kai and Tomita, 1979; Tomita 1982; and references therein) as well as Lin and coworkers (Hao and Zhang, 1982; Hao et al., 1983), and recently the author and coworkers (Kevrekidis et al., 1986*a*; Aronson et al., 1986) have studied the interaction of the natural oscillation with the external forcing in terms of what we call excitation diagrams. These are two-parameter diagrams describing the qualitative behavior of the system as a function of the forcing amplitude α and the forcing frequency ω (more appropriately the ratio ω/ω_0). We examine here global phenomena that cause the creation or annihilation of quasiperiodic (multifrequency) oscillatory responses. Such phenomena are by no means particular to our trial system. We have observed them also in test cases including a simple surface reaction scheme (Kevrekidis et al., 1986*a*) as well as the forced CSTR (Kevrekidis et al., 1986*b*), and we expect them to be present in a large class of forced oscillatory and three-dimensional autonomous systems and maps. The current example, however, is the one that provided the most representative illustrations, while the computational work was easier, the equations not being stiff.

Simple Frequency Locking on a Torus

Frequency locking (entrainment) is an important nonlinear phenomenon in the study of forced oscillators. When it occurs, the system develops periodic responses whose periods are exact integer multiples of the period of the forcing; we say that the forcing has entrained the system (Hayashi, 1964; Minorsky, 1962). We study the forced Brusselator at $\alpha = 0.0005$ as ω/ω_0 is varied. At $\omega/\omega_0 = 0.988$ the system has a stable quasiperiodic solution that winds around a toroidal (doughnut-shaped) surface in phase space. Viewed stroboscopically, this appears as an attracting closed curve—an invariant circle *IC*, Figure 8a. The phase point hops along this curve discontinuously in a clockwise fashion without ever returning to the same point precisely. In the interior of this closed curve lies an unstable focus $U\Phi$ fixed point, representing an unstable oscillation with the same period as the forcing term. Computationally, the invariant circle can be

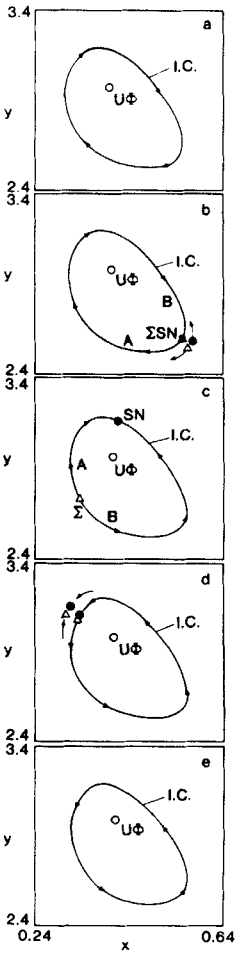

Figure 8. Stroboscopic sections illustrating frequency locking on a torus.

found by solving a nonlinear functional equation (Kevrekidis et al., 1985). At $\omega/\omega_0 = 0.98910245$ the quasiperiodic solution suddenly disappears. A fixed point ΣSN appears on the invariant circle (representing an oscillation on the torus). This is a saddle-node point, and at the moment it appears it is marginally stable ($\lambda_1 = 1$, $\lambda_2 < 1$). For larger values of ω/ω_0 the saddle Σ and the node SN move apart on the circle, Figure 8c, which retains its integrity and its smoothness. It now consists of the two arms, ΣA and ΣB, of the unstable manifold of the saddle Σ with the stable node SN.

This phenomenon, involving the loss of a quasiperiodic oscillation is of course a global phenomenon. Not only the emerging periodic oscillations (Σ and SN) but also the invariant manifolds—$(\Sigma SN)A$ and $(\Sigma SN)B$ of the saddle node ΣSN in Figure 8b, and ΣA and ΣB of the saddle Σ in Figure 8c—are involved in the annihilation of the multifrequency response. The loop $\Sigma A(SN)B\Sigma$ characterizes the "globality" of the phenomenon, since it is not confined near the fixed points Σ and SN, but travels far away from them in phase space. Even though the phenomenon is global, it is possible to find it by local methods. The onset of this behavior involves a saddle-node bifurcation, and we can compute this saddle node independently of the entire loop. This is obtained by appending the equation

$$\lambda_1(\omega/\omega_0) - 1 = 0 \qquad (13)$$

to an algorithm for finding periodic orbits. We thus find the particular value of the parameter ω/ω_0 for which this condition is satisfied (Kevrekidis et al., 1986b). It is of course significant that we know (*a priori*, through simulations, through perturbation techniques) that our system exhibits frequency locking, since not every saddle-node bifurcation will produce (or destroy) a quasiperiodic response. A case in which this does not happen is illustrated later.

This phenomenon is very similar to the Andronov-Leontovic case II presented in part I, where a limit cycle was destroyed by the appearance of a saddle-node steady state on it. In that case, the unstable manifold branches of the saddle steady state that destroyed the limit cycle were simple trajectories, not families of trajectories. For the sake of completeness, we add that as ω/ω_0 varies further, the saddle Σ and the node SN move further apart, and the counterclockwise arm ΣB of the unstable manifold of Σ grows at the expense of the clockwise arm ΣA-Figure 8d. When Σ and SN meet again in another saddle node bifurcation at $\omega/\omega_0 = 1.01203499$ they annihilate each other, and we are left with a quasiperiodic oscillation winding around the torus surface (the phase point now moves in a counterclockwise fashion on the invariant circle). We conclude that this mechanism of formation (and loss) of quasiperiodic attractors, although a global phenomenon, can be found through algorithms utilizing local information.

Period 1: Homoclinic Tangencies and Crossings

In a different set of numerical experiments we set $\alpha = 0.0055$ and vary the forcing frequency around $\omega/\omega_0 = 0.9$. Initially the system has a smooth, globally attracting invariant circle IC (an attracting torus) surrounding an unstable focus periodic point $U\Phi$. This point lies on an unstable oscillation that has the same period as the forcing, and its two free characteristic multipliers are complex conjugate and have norm greater than 1 (a complex source, Figure 9a, $\omega/\omega_0 = 0.905$, $\lambda_{1,2} = 0.72399 \pm 1.013794\,i$,

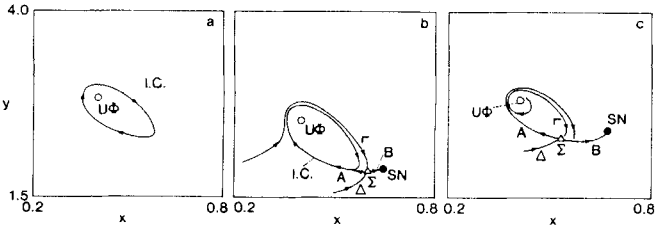

Figure 9. Stroboscopic phase planes taken as forcing frequency ω of a forced Brusselator is varied.
(b) shows two coexisting attractors, one periodic, one quasiperiodic

where $|\lambda_{1,2}| = 1.24577$). At $\omega/\omega_0 = 0.906734776$, however, a saddle node appears outside the invariant circle, and as ω/ω_0 changes further the saddle Σ moves away from the stable node SN, Figure 9b. This means that stable periodic (SN) and stable quasiperiodic (IC) oscillations coexist for these parameter values. Figure 9b also provides us with a good example of a saddle-node bifurcation of periodic solutions that does not involve destruction of the quasiperiodic orbit. The two branches ΣA and ΣB of the unstable manifold $W^u(\Sigma)$ of the saddle point Σ do not form a loop. Instead, they become attracted, each by one of the two existing attractors: ΣA by the invariant circle and ΣB by the stable node. The two arms $\Sigma\Gamma$ and $\Sigma\Delta$ of the stable manifold $W^s(\Sigma)$ of the saddle point provide the separatrix of the basins of attraction between the two attractors.

As we change ω/ω_0 further, the invariant circle IC grows and approaches the saddle Σ, while the arm $\Sigma\Gamma$ of the stable manifold hugs IC closer and closer. It is evident that we are approaching some type of homoclinic breaking of the torus (homoclinic because it involves invariant manifolds of one and the same saddle point). If we take a coarse step forward in ω/ω_0, we will find the situation depicted in Figure 9c ($\omega/\omega_0 = 0.91$). $\Sigma\Gamma$ and ΣA have crossed, the invariant circle has been destroyed, only one attractor (the stable node SN) exists, and both branches ΣA and ΣB of the unstable manifold are attracted to it. $\Sigma\Gamma$ now winds around the unstable period 1 ($U\Phi$) as time (actually n, the number of iterates of the map) tends to $-\infty$. The sequence of Figures 9a, 9b, and 9c is reminiscent of what we encountered in Figures 1 and 5. The torus in Figure 9b, however, is not broken by a mechanism similar to an infinite-period bifurcation in a two-dimensional system. The difference between two-dimensional maps and two-dimensional ODE's (flows) comes into play. The unstable ΣA and stable $\Sigma\Gamma$ manifolds of the saddle Σ cannot coincide as happens in the ODE case; the closest that they can come together is to be quadratically tangent to each other (Newhouse, 1980).

In Figure 10a ($\omega/\omega_0 = 0.901805$) ΣA and $\Sigma\Gamma$ are coming quite close to each other before $\Sigma\Gamma$ escapes to infinity. The first visible indication of strange behavior appears in Figure 10b ($\omega/\omega_0 = 0.901815$). $\Sigma\Gamma$ develops a small "bump" that becomes more pronounced. When we come to Figure 10c ($\omega/\omega_0 = 0.908151$) $\Sigma\Gamma$ has developed an infinite sequence of (quadratic) tangencies to ΣA. These tangencies do not start suddenly at E, they only start becoming visible in the scale of Figure 10c at E. More can be found by iterating E forward and backward under the map. E and its iterates are homoclinic points. They belong to both the stable and the unstable manifold of the saddle. As ω/ω_0 changes further, the manifolds cross each other as the points of tangency of Figure 10c move upward through ΣA (Figure 10d, $\omega/\omega_0 = 0.908152$, and Figure 10e, $\omega/\omega_0 = 0.908153$). We say

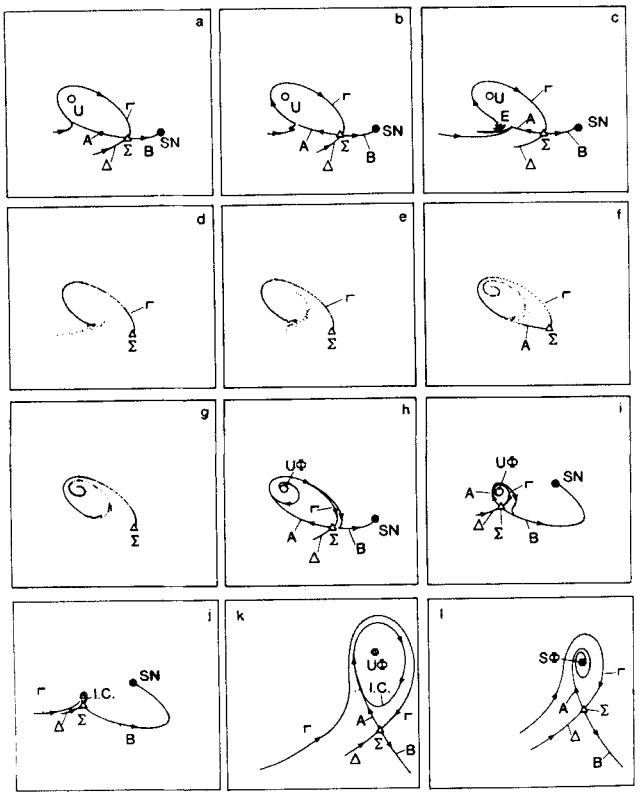

Figure 10. Stroboscopic phase plane details of transition from Figure 9B to Figure 9c.

that we have an infinity of transversal intersections between the stable and unstable manifolds. That erratic behavior, chaos, infinities of attractors, and Smale horseshoes lie in the vicinity of such pictures as Figure 10d, and Figure 10e is the subject of a number of theorems in the theory of dynamical systems (Newhouse, 1979, 1980; Smale, 1964, 1967). We have not yet searched in our example for details of such nontrivial dynamics. Infinities of crossing points exist all along ΣA and $\Sigma\Gamma$. In the same fashion that $\Sigma\Gamma$ becomes erratic by folding and oscillating vigorously in a direction roughly parallel to $\Delta\Sigma\Gamma$ as it approaches Σ, ΣA also becomes erratic as it approaches Σ from the $\Sigma\Gamma$ side. It also folds and oscillates vigorously in a direction roughly parallel to $A\Sigma B$. These folds however lie so close to the saddle and to $A\Sigma B$ that it is not possible to resolve them and still be able to see the entire loop in the same picture. The folds of $\Sigma\Gamma$ intersect then again and again with the folds of ΣA and the result is a very complicated structure called appropriately a homoclinic tangle. Descriptions of tangles and ways of disentangling them can be found in Abraham and Shaw (1985, part III) and Smale (1964). We reiterate that the saddle manifolds we observe on the Poincaré plane II are not trajectories, but rather one-parameter families of trajectories (they actually fill surfaces whose intersections with II constitute ΣA and $\Sigma\Gamma$). A point such as E and its forward and backward iterates lie on a single trajectory. This trajectory belongs to both the stable and the unstable manifold surfaces of the oscillation. The intersection of the manifold surfaces consists of a trajectory or trajectories that belong to both surfaces.

As we further vary ω/ω_0 we come to Figure 10f ($\omega/\omega_0 = 0.9081535$). The manifolds have gone completely through each other and we now have a homoclinic tangency from the inside. After this value of ω/ω_0 the behavior of the manifolds becomes normal again. Some remnants of the homoclinic tangle can still be seen in the winding approach of $\Sigma\Gamma$ toward $U\Phi$ iterated backward in Figure 10g ($\omega/\omega_0 = 0.9081540$). In Figure 10h ($\omega/\omega_0 = 0.91$) the situation appears the same as in Figure 9c: the homoclinic storm has abated, and the manifolds appear smooth.

It should be evident that any attempt to accurately locate the parameter values for which the homoclinic tangency occurs is not an easy task. In fact, Figures 9 and 10 have been obtained by brute force through simulation, not through fixed point algorithms. The method used to obtain these figures is a modification of the code used in Aronson et al. (1982) as follows: The saddle point Σ is found by a Newton-Raphson iteration on a shooting algorithm for the computation of periodic orbits. An approximation to the local stable and unstable manifolds is then constructed, consisting of segments of the eigenvectors of the linearization of the stroboscopic map around Σ. A (large) number of initial conditions are taken on this manifold segment (we need an entire family of trajectories) and all these initial conditions are iterated, forward and backward. We thus obtain approximations to the global unstable and stable manifolds respectively.

We are currently working on an algorithm that is capable of converging iteratively on the value of the parameter for which the homoclinic tangency first occurs (at which point the invariant circle and the torus it represents are lost). It consists of computing a finite initial segment of the stable and unstable manifolds, and imposes the condition that these segments are tangent at some point. It is precisely this boundary condition that will be satisfied at the homoclinic tangency point, and that will provide us with the equation to be solved for the corresponding parameter value. The fact that an infinity of tangencies exist along the entire length of the manifolds is resolved by working with finite manifold segments and thus concentrating on the first time that they cross. We will return to this algorithm on another occasion.

Dynamic behavior similar to the type described above is by no means novel. It is actually quite standard in the study of maps of the plane, and hence Poincaré maps of three- and higher dimensional ODE's. The above presentation serves first to complete the picture described for two-dimensional systems, and gives us a chance to contrast two- and three-dimensional homoclinicity. Second, our case study provides a nice illustrative example. Although the transition from Figure 9b to Figure 9c can easily be observed in the dynamics of several systems, actually obtaining the sequence of Figure 10a to Figure 10h from a given system is practically difficult. In our experience, the folding of the manifolds becomes so compressed close to the saddle that they are extremely difficult to see, even if one knows that they are there. In Figure 10d, for example, all the folds of ΣA are so close to $A\Sigma B$ that even in a tenfold magnification of the figure close to Σ they are not visibly separate from $A\Sigma B$. Nevertheless, observation of a transition such as the one from Figure 9b to Figure 9c necessarily implies that all of the sequence of Figure 10 occurs in between, whether easily visible or not. One can show that such phenomena will occur as a torus-breaking mechanism in almost every periodically forced oscillator, and also in autonomous systems. In a recent experimental paper the author and his coworkers have discovered this sequence of events in a Rayleigh-Bénard autonomous convection experiment (Ecke et al., 1987). The

operating significance of such a complex sequence of events is clear: it signals the hysteretic coexistence of periodic and quasi-periodic responses (before the bifurcation). After the bifurcation we have only one attractor, the periodic oscillation SN. Finally, our example demonstrates how close simple systems are to complicated temporal behavior (horseshoes, infinity of attractors, etc.).

For the sake of completeness we add that in the above model, as we further vary ω/ω_0 the procedure reverses itself. A new homoclinic sequence of tangency-crossing-tangency occurs, $\Sigma\Gamma$ and ΣA cross again in the opposite direction, and this now gives birth to a stable quasiperiodic oscillation (an invariant circle *IC*, Figure 10j and enlargement, Figure 10k, $\omega/\omega_0 = 0.936$). This circle subsequently shrinks an collapses on $U\Phi$ (which then becomes stable, $S\Phi$) in a Hopf bifurcation of a limit cycle to a torus (Figure 10l, $\omega/\omega_0 = 0.9375$). The latter case is a typical local bifurcation to a quasiperiodic oscillation, as opposed to its global birth signalled by the homoclinic tangle that we examined above. We do not precisely know at what parameter value the torus stops existing, nor how exactly it loses smoothness as we approach the onset of the homoclinic tangle. We do know however that once the homoclinic tangency is observed, the torus exists no more.

Period 3

The homoclinic scenario just presented provides a nice framework in which to explain certain phenomena observed in the high forcing amplitude region of an excitation diagram (regions of strong resonance). In this section we examine transformations of the stroboscopic phase plane that occur as we change one operating parameter, the forcing amplitude α or the forcing frequency ω/ω_0. These transformations involve homoclinic manifold interactions. They are crucial in determining the structure of resonance regions (the limits of entrainment). We choose a period 3 resonance of the forced Brusselator to illustrate these phenomena. It is a basic result that for small forcing amplitude the entrainment region will appear shaped like a wedge with its tip at $\omega/\omega_0 = 3$, Figure 11a. The boundaries of the region are loci of saddle-node bifurcations where the (subharmonic) period 3 points are formed and annihilated. For small α we observe frequency locking on a torus (a global manifold loop) as described previously. When the operating conditions are chosen at point *A*, Figure 11a, the phase plane exhibits a single attracting invariant circle. As ω/ω_0 varies, at the boundary of the resonance three saddle nodes appear on the invariant circle and the quasiperiodic oscillation is lost. They then separate to three saddles Σ_i ($i = 1, 2, 3$) and three nodes SN_i. The loop now consists of the union of both arms of the unstable manifolds of all three saddles with the three nodes. As we cross the resonance region (changing ω/ω_0) the periodic points on the circle rotate, and at the righthand side boundary we again have a set of three saddle-node bifurcations. The coupling of the saddles with the nodes however has changed from $\Sigma_1 SN_1$, $\Sigma_2 SN_2$, $\Sigma_3 SN_3$ to $\Sigma_1 SN_2$, $\Sigma_2 SN_3$, and $\Sigma_3 SN_1$, as shown in the bifurcation diagram, Figure 11c. At some higher amplitude however, say $\alpha = 0.0055$, a significant change is observed. If the operating conditions are chosen at point *D*, Figure 11a, we observe qualitatively the same behavior as at point *A*: the invariant circle still exists and is attracting. At a point such as *F*, however, the subharmonic period 3 points have been born off the invariant circle like satellites, Figure 11d. The quasiperiodic response has not been destroyed, but it coexists with a

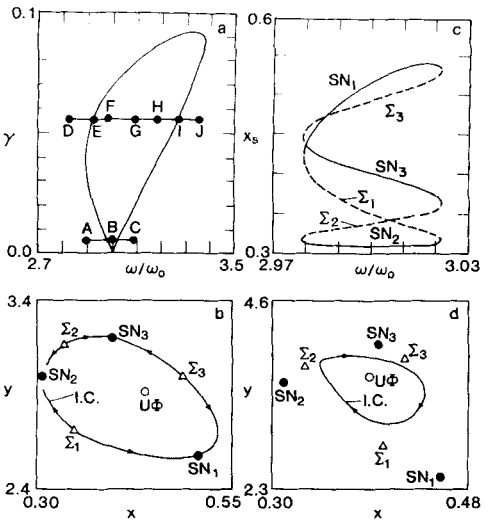

Figure 11. (a) Two distinct one-parameter cuts across a resonance region.
(b) Phase plane for *ABC* in (a).
(c) Bifurcation diagram showing change from (b) to (d) in pairing of saddles and nodes.
(d) Phase plane for *DEFGHIJ* in (a).

stable period 3 oscillation. The stable manifolds $\Sigma_i\Gamma_i$ and $\Sigma_i\Delta_i$ of the saddles Σ_i constitute the separatrices between the regions of attraction of the three stable period 3 points (that represent a period 3 oscillation) and the invariant circle (representing a quasiperiodic oscillation, Figure 12a). The two issues we address are:

1. The change in the saddle-node pairing between points *E* and *I* in Figure 11a: Does the invariant circle (and the underlying quasiperiodic oscillation) persist along the entire semgent *DJ*?

2. The feasibility of a smooth, continuous change of the phase plane from Figure 12a to a global manifold loop (a frequency-locked torus) in Figure 11b. In other words, how all six periodic

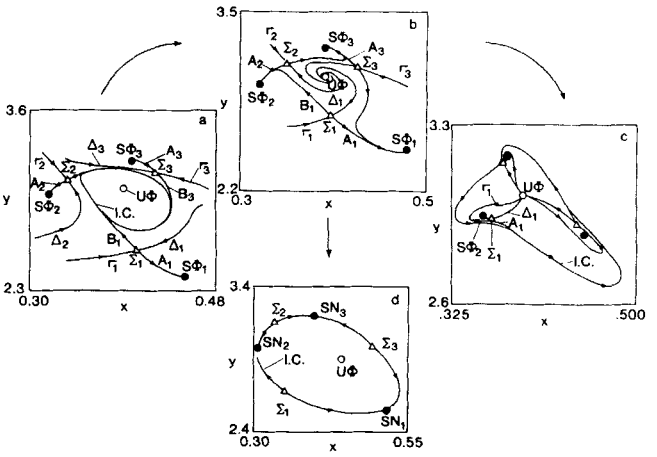

Figure 12. Stroboscopic phase planes at different points of Figure 11a.
(a) *F*, Figure 11a; (b) *G*, Figure 11a; (c) *H*, Figure 11a; (d) *B*, Figure 11a
Note destruction and reformation of a torus in (a)–(b)–(c) transition

points off the circle in Figure 12a can get on the circle in Figure 11b while simultaneously destroying the quasiperiodic oscillation.

Exchanging partners

We describe the changes occurring through the path *DEFGHIJ*, Figure 11a. At F the invariant circle has the same rotation orientation as at D. The saddles Σ_i and the nodes SN_i were born in pairs at point E ($\omega/\omega_0 = 2.92015618$). Soon after E the stable periodic points SN_i change from nodes to foci $S\Phi_i$ (their characteristic multipliers become complex conjugate, but with norm less than 1). This does not cause any change in the phase plane, although its qualitative importance will be made apparent later. The unstable manifold arms $\Sigma_i A_i$ are attracted by the stable foci $S\Phi_i$, while the branches $\Sigma_i B_i$ are attracted to the invariant circle *IC*, Figure 12a. Changing ω/ω_0 causes the invariant circle to grow and brings it close to the branches $\Sigma_i\Delta_i$ of the stable manifolds of the saddles. Then, through a sequence of homoclinic tangency-crossing-tangency, the branches $\Sigma_i\Delta_i$ cross the corresponding branches $\Sigma_{i-1}B_{i-1}$ (the indices $i = 1, 2, 3$ are taken cyclically) and the invariant circle is lost (along with the underlying quasiperiodic oscillation). We call this procedure homoclinic, not heteroclinic, because all the saddles Σ_i lie on the same period 3 oscillatory trajectory of the full system, and the manifolds themselves are cyclic stroboscopic images of each other. That is, if $f^{(i)}(S)$ is the ith stroboscopic iterate of a point S, then

$$\Sigma_3\Delta_3 = f(\Sigma_2\Delta_2) = f^{(2)}(\Sigma_1\Delta_1) = f^{(3)}(\Sigma_3\Delta_3) \qquad (14)$$

Had we considered the third iterate of the map, however, each of the periodic points would become an individual fixed point, and the crossings could be considered heteroclinic. This means that the sequence of pictures we observe here will be qualitatively the same in the case of heteroclinic crossings.

The picture now has changed to Figure 12b. The stable manifolds $\Sigma_i\Delta_i$ are attracted backward by the unstable focus $U\Phi$ now that the invariant circle is broken. Observe that the unstable manifold arms $\Sigma_i B_i$ are now attracted to the next (cyclically) attracting point $S\Phi_{i+1}$. This is one-half of the step necessary for the saddles and nodes to exchange partners between E and I. The next step must detach the $\Sigma_i A_i$ from the old attractors $S\Phi_i$, and in the process somehow reinstate the invariant circle. This can be seen in the sequence of Figures 12a, 12b, and 12c. The homoclinic scenario is slightly modified: the $\Sigma_i A_i$ branches now cross the $\Sigma_{i-1}\Gamma_{i-1}$ (the indices are always taken cyclically) and the result is shown in Figure 12c. Both sides of the stable manifolds $\Sigma\Gamma$ and $\Sigma\Delta$ of the saddles Σ now go to the unstable focus period 1 $U\Phi$ inside the torus. The invariant circle (and hence the quasiperiodic oscillation) has been reinstated, but now it surrounds the periodic solutions. Every initial condition on the stroboscopic phase plane eventually gets attracted to the invariant circle, except for the interiors of the three clover leaves formed by the $\Sigma_i\Gamma_i$ and $\Sigma_i\Delta_i$ that constitute the basins of attraction of the stable oscillation $S\Phi_i$. The exchange of partners from $\Sigma_i - S\Phi_i$ to $\Sigma_i - S\Phi_{i+1}$ has been accomplished in these two steps, and the invariant circle has been destroyed and reformed (with different rotation orientation) in the process.

Soon afterward, the stable foci become stable nodes again, approach the saddles, and annihilate them in a new saddle-node bifurcation that marks the righthand-side boundary of the entrainment region and leaves us with an invariant circle as the only attractor on the Poincaré plane II.

Changing sides

We now examine the transition from a phase plane picture like Figure 12a (point F in Figure 11a) to a frequency-locked picture like Figure 11b (point B in Figure 11a). In other words, we examine the transitions that bring the entrained subharmonic solutions onto the invariant circle when they are created off it. In this process a quasiperiodic oscillation is destroyed in a way that differs from simple frequency locking. Understanding this is greatly facilitated by our previous discussion. Consider the path *FGB* in Figure 11a. The invariant circle breaks in the process of a homoclinic bifurcation and we obtain Figure 12b. The loop $\Sigma_1(S\Phi_2)\Sigma_2(S\Phi_3)\Sigma_3(S\Phi_1)\Sigma_1$ has essentially the same structure as the smooth circle in Figure 11b. The only difference is that the latter loop is smooth, while the former has infinite spirals at the three focus points $S\Phi_i$. The only change necessary to go from one loop to another is to change the foci $S\Phi$ to nodes SN along the line GB, a process that does not involve any loss of stability. The unstable manifold arms $\Sigma_i A_i$ approach the node SN_{i-1} tangent to one side of its "weak" eigendirection (the eigenvector corresponding to the largest eigenvalue of the linearization), while the unstable manifold arm $\Sigma_{i-1}B_{i-1}$ of the next saddle will approach SN_{i-1} from the other side of its weak stable eigendirection, thus restoring the smoothness of the invariant circle.

Discussion and Conclusions

In this paper we have studied certain aspects of the numerical computation of global bifurcations. In part I we discussed infinite-period bifurcations in systems with two degrees of freedom. We presented two algorithms developed for this purpose. The first, the invariant curve method, is a special case of invariant manifold computation applied to the two-dimensional infinite-period bifurcation scenario. The second is our double-shooting implementation of Hassard's algorithm. We have illustrated both algorithms using several simple systems of chemical engineering interest. As Keener (1981) succintly discusses, these phenomena are to be expected in systems with S-shaped steady solution diagrams for which Hopf bifurcations are possible; in other words, in systems that may possess steady states with a double zero eigenvalue (Bogdanov, 1975; Guckenheimer and Holmes, 1983). A nice experimental observation of such a point as well as of the infinite-period oscillations close to it for an electrochemical system can be found in Pismen and Lev (1986). Close to such a point, analytical techniques can be used to compute the infinite-period bifurcation. Our intention was to present numerical methods applicable even away from such special points in parameter space, adaptable easily enough (at least conceptually) to the computation of heteroclinic orbits and saddle-node separatrices. Such techniques are also applicable as auxiliary tools in the study of higher dimensional systems through the method of averaging (Greenspan and Holmes, 1984) to calculate the limits of validity of the averaging approximation.

For the sake of completeness, we mention the way E. J. Doedel has implemented the detection of an infinite period bifurcation in his package AUTO (Doedel, 1981). In the continuation of limit cycle branches, the period T of the limit cycle is explicitly solved for and used to normalize the solution from 0 to 1 instead of from 0 to T. The period also contributes to the norm

of the solution used in the bifurcation diagrams. AUTO detects an infinite-period bifurcation essentially when the period becomes very large. Its power lies in that due to the adaptive discretization it can calculate accurate limit cycles even when the period T is very large (when other methods would produce spurious solutions or fail to converge) and thus approximate the homoclinic point better. In essence, AUTO does not find homoclinic orbits, but can approximate them adequately for some purposes.

In part II we examined global bifurcations commonly observed in systems described by both autonomous (at least three) and periodically forced (at least two) nonlinear coupled ordinary differential equations. In particular, we concentrated on such phenomena as involve the creation and annihilation of multifrequency responses. We found that this type of transition often involves hetero- and homoclinic (global) manifold interactions and tangles, along with the erratic behavior they imply. We have observed such phenomena in several trial systems. Furthermore, we expect them to be present in the dynamics of large classes of systems, both physical and chemical, that involve resonances, particularly in periodically forced systems. We find it bewildering that such complicated phenomena appear commonplace in the dynamics of simple systems. We believe that this ubiquitousness justifies their study and, more concretely, the development of algorithms for their accurate numerical computation. We have described the foundations of an algorithm for the computation of homoclinic tangencies; this is the focal point of our current research. We believe that such algorithms—special cases of which have started appearing in the literature (Tel, 1983)—will be important in the study and modeling of chemical dynamics, and more generally of dynamical systems, since the phenomena they address are quite difficult and often impossible to locate and unravel just through simulations. In fact, such phenomena are usually studied in the literature only for systems whose trajectories can be explicitly found or approximated.

Through our trial example we presented some features of the qualitative structure of resonance regions and their boundaries. The work of Aronson et al. (1982) shows an entire spectrum of such features involving global manifold interactions for maps. We have been working jointly with them (Aronson et al., 1986a) on the numerical study and classification of such phenomena that are common to maps and to Poincaré sections of ordinary differential equations. We also discussed the apparent similarities and highlighted the differences of related phenomena in the case of two-dimensional ODE's and two-dimensional Poincare sections of three-dimensional systems.

This paper has been extensively descriptive in an attempt to provide the uninitiated with enough diagrams to understand the raison d'etre of the algorithms, grasp their underlying principles, and appreciate the importance as well as the ubiquitousness of the phenomena. We hope that we have also furnished the chemical dynamics researcher with useful tools for the numerical study of these phenomena. We believe that numerical techniques like the invariant curve method with appropriate additional conditions can be extended to the study of homoclinicity and heteroclinicity in higher dimensional systems. We are currently working on such extensions as well as on connecting our numerical results with analytical work close to points with a double zero eigenvalue and with Mel'nikov methods. We also think that recent efforts (Abraham and Shaw, 1985) to provide visual instructional material describing such dynamics are very helpful in guiding the nonmathematician scientist toward understanding their phenomenological structure.

We believe that knowledge of the detailed structure of global phenomena is necessary in order to pose them as numerical problems for which algorithms can be constructed. This will enhance our understanding of the phenomena and their implications in chemical dynamics and our capability of designing experiments in order to probe the resulting behavior; and it will eventually make us capable of routinely analyzing the dynamics of case studies of interest.

Acknowlegments

We thank R. Aris, L. D. Schmidt, R. P. McGehee, and D. G. Aronson for helpful discussions. This work was partially supported by National Science Foundation Grant No. CPE 83-13497, and was performed under the auspices of the U.S. Department of Energy.

Notation

A, B, a, b, y_o, k = parameters
IC = invariant circle (Poincaré section of a torus)
LC = limit cycle
SN (SF) = stable node (focus) steady state
SN ($S\Phi$) = stable node (focus) oscillatory solution
S = saddle-type steady state
SA, SB = unstable manifold branches of saddle steady state
SC, SD = stable manifold branches of saddle steady state
t, T = time
UN (UF) = unstable node (focus) steady state
UN ($U\Phi$) = unstable node (focus) oscillatory solution
$W(\cdot)$ = invariant manifold of saddle-type steady state or limit cycle
x, y, x_i, y_i, u_i, v_i = variables

Greek letters

$\alpha, \beta, \gamma, \delta$ = parameters
θ = residence time; submonolayer coverage
λ = eigenvalues of linearization (Floquet multipliers for limit cycles)
Π = stroboscopic section
Σ = saddle-type limit cycle
$\Sigma A, \Sigma B$ = unstable manifold branches of saddle limit cycle
$\Sigma\Gamma, \Sigma\Delta$ = stable manifold branches of saddle limit cycle
$\omega(\omega_0)$ = forcing (natural) frequency

Subscript

h = homoclinic

Superscripts

s = stable (manifold)
u = unstable (manifold)

Literature Cited

Abraham, R. H., and C. D. Shaw, *Dynamics, the Geometry of Behavior;* I: *Periodic Behavior,* II: *Chaotic Behavior,* III: *Global Behavior,* Aerial Press, Santa Cruz, NM (1985).

Andronov, A. A., E. A. Leontovic, I. I. Gordon, and A. G. Maier, *Theory of Bifurcations of Dynamical Systems on a Plane* (trans. from Russian, 1967), Israel Prog. for Sci. Trans., Jerusalem (1971).

Arnol'd, V. I., *Ordinary Differential Equations* (trans. from Russian by R. A. Silvermann), M.I.T Press (1973).

Aronson, D. G., "Lectures on the Porous Media Equation," *CIME Lectures on Nonlinear Diffusion* A. Fasano, ed., *Lect. Notes in Math,* Springer, New York (1986).

Aronson, D. G., M. A. Chory, G. R. Hall, and R. P. McGehee, "Bifurcations from an Invariant Circle for Two-Parameter Families of Maps of the Plane: A Computer-Assisted Study," *Comm. Math. Phys.* **83,** 303 (1982).

Aronson, D. G., R. P. McGehee, I. G. Kevrekidis, and R. Aris, "Entrainment Regions for Periodically Forced Oscillators," *Phys. Rev. A*, **33**, 2190 (1986a).
Aronson, D. G., E. Doedel, and H. G. Othmer, "An Analytical and Numerical Study of the Bifurcations in a System of Linearly Coupled Oscillators," *Physica D*, (1986b).
Balakotaiah, V., and D. Luss, "Global Analysis of the Multiplicity Features of Multi-Reaction Lumped Parameter Systems," *Chem. Eng. Sci.*, **39**, 865 (1984).
Bendixson, I., "Sur les Courbes Definies par des Equations Differentielles," *Acta Math.*, **24** (1901).
Bogdanov, R. I., "Versal Deformations of a Singular Point on the Plane in the Case of Zero Eigenvalues," *Funct. Anal. Appl.*, **9**, 144 (1975).
Doedel, E. J., "AUTO: A Program for the Automatic Bifurcation Analysis of Autonomous Systems," *Cong. Num.*, **30**, 265 (1981).
Dulac, H., "Sur les Cycles Limites," *Bull. Soc. Math. France*, **51**, 45 (1923).
Ecke, R. E., and I. G. Kevrekidis, "Interactions of Resonances and Global Bifurcations in Rayleigh-Bénard Convection," submitted, *Phys. Lett.*, A (1987).
Farr, W. W., and R. Aris, " 'Yet Who Would Have Thought the Old Man to Have Had so Much Blood in Him?' Reflections on the Multiplicity of Steady States of the Stirred-Tank Reactor," *Chem. Eng. Sci.*, **41**, 1385 (1986).
Golubitsky, M., and D. G. Schaeffer, *Singularities and Groups in Bifurcation Theory*, Vol. 1, Springer Verlag, New York (1985).
Greenspan, B., and P. J. Holmes, "Repeated Resonance and Homoclinic Bifurcation in a Periodically Forced Family of Oscillators," *SIAM J. Math. Anal.*, **15**, 69 (1984).
Gray, P., and S. K. Scott, "Autocatalysis in Isothermal, Open Systems," *J. Chem. Phys.*, **79**, 6421 (1983).
———, "Autocatalytic Reactions in the Isothermal Continuous Stirred-Tank Reactor: Oscillations and Instabilities in the System $A + 2B \rightarrow 3B$, $B \rightarrow C$," *Chem. Eng. Sci.*, **39**, 1087 (1984).
Guckenheimer, J., and P. J. Holmes, *Nonlinear Oscillations, Dynamical Systems and Bifurcations of Vector Fields*, Springer, New York (1983).
Hao, B. L., and S.-Y. Zhang, "Hierarchy of Chaotic Bands," *J. Stat. Phys.*, **26**, 769 (1982).
Hao, B. L., G. R. Wank, and S.-Y. Zhang, "U-sequences in the Periodically Forced Brusselator," *Comm. Theor. Phys.*, **2**, 1075 (1983).
Hassard, B. D., "Computation of Invariant Manifolds," *New Approaches to Nonlinear Problems in Dynamics*, P. J. Holmes, ed., SIAM, 7 (1980).
Hassard, B. D., N. D. Kazarinoff, and Y.-H. Wan, *Theory and Applications of Hopf Bifurcation, London Math. Soc. Lect. Note Series*, **41**, Cambridge (1981).
Hayashi, C., *Nonlinear Oscillations in Physical Systems*, McGraw Hill, New York (1964).
Hirsch, M. W., C. C. Pugh, and M. Schub, *Invariant Manifolds, Lecture Notes in Mathematics*, **583**, Springer, New York (1977).
Iooss, G., and D. D. Joseph, *Elementary Stability and Bifurcation Theory*, U.T.M. Series, Springer, New York (1980).
Jorgensen, D. V., W. W. Farr, and R. Aris, "More on the Dynamics of the Stirred Tank with Consecutive Reactions," *Chem. Eng. Sci.*, **39**, 1741 (1984).
Kai, T., and K. Tomita, "Stroboscopic Phase Portrait of a Forced Nonlinear Oscillator," *Prog. Theor. Phys.*, **61**, 54 (1979).
Keener, J. P., "Infinite Period Bifurcation and Global Bifurcation Branches," *SIAM J. Appl. Math.*, **41**, 127 (1981).
Kevrekidis, I. G., L. D. Schmidt, and R. Aris, "On the Dynamics of Periodically Forced Chemical Reactors," *Chem. Eng. Comm.*, **30**, 323 (1984).
Kevrekidis, I. G., R. Aris, L. D. Schmidt, and S. Pelikan, "The Computation of Invariant Circles of Maps," *Physica D.*, **16**, 243 (1985).
Kevrekidis, I. G., L. D. Schmidt, and R. Aris, "Some Common Features of Periodically Forced Reacting Systems," *Chem. Eng. Sci.*, **41**, 1263 (1986a).
———, "The CSTR Forced," *Chem. Eng. Sci.*, **41**, 1549 (1986b).
Krylov, N. M., and N. N. Bogoliubov, *Introduction to Nonlinear Mechanics*, Princeton (1947).
Kubicek, M., and M. Marek, *Computational Methods in Bifurcation Theory and Dissipative Structures*, Springer Verlag, New York (1983).
Minorsky, N., *Nonlinear Oscillations* Van Nostrand, New York (1962).
Muskat, M., *The Flow of Homogeneous Fluids Through Porous Media*, McGraw-Hill, New York (1937).
Newhouse, S. E., "The Abundance of Wild Hyperbolic Sets and Nonsmooth Stable Sets for Diffeomorphisms," *Publ. IHES*, **50**, 101 (1979).
———, *Lectures on Dynamical Systems, Progr. Math.*, **8**, Birkhauser, Boston (1980).
Othmer, H. G., D. G. Aronson, and E. J. Doedel, "Resonance and Bistability in Coupled Oscillators," *Phys. Lett.*, **113A**, 349 (1986).
Pismen, L. M., "Kinetic Instabilities in Man-made and Natural Reactors," *Chem. Eng. Sci.*, **35**, 1950 (1980).
———, "Methods of Singularity Theory in the Analysis of Dynamics of Reactive Systems," *Reacting Flows: Combustion and Chemical Reactors, Am. Math. Soc. Lect. Appl. Math*, **24**, G. S. S. Ludford, ed. (1986).
Pismen, L. M., and O. Lev, "Oscillatory Dynamics of Nickel Dissolution," *Paper no. 78G*, AIChE Ann. Meet., Miami (Nov., 1986).
Seydel, R., "Numerical Computation of Periodic Orbits that Bifurcate from Stationary Solutions of Ordinary Differential Equations," *Appl. Math. Comput.*, 257 (1981).
Schwartz, I. B., "Estimating Regions of Existence of Unstable Periodic Orbits Using Computer-Based Techniques," *SIAM J. Num. Anal.*, **20**, 106 (1983).
Smale, S., "Diffeomorphisms with Many Periodic Orbits," *Differential and Combinatorial Topology Symposium in Honor of Marston Morse*, Princeton (1964).
———, "Differentiable Dynamical Systems," *Bull. Am. Math. Soc.*, **73**, 747 (1967).
Tel, T., "On the Construction of Invariant Curves of Period Two Points in Two-Dimensional Maps," *Phys. Lett.*, **94A**, 334 (1983).
Tomita, K., "Chaotic Response of Nonlinear Oscillators," *Phys. Rep.*, **86**, 113 (1982).
Takoudis, C. G., L. D. Schmidt, and R. Aris, "Isothermal Sustained Oscillations in a Very Simple Surface Reaction," *Surf. Sci.*, **105**, 325 (1981).
Uppal, A., W. H. Ray, and A. B. Poore, "On the Dynamic Behavior of Continuous Stirred-Tank Reactors," *Chem. Eng. Sci.*, **29**, 967 (1974).
———, "The Classification of the Dynamic Behavior of Continuous Stirred-Tank Reactors—Influence of the Reactor Residence Time," *Chem. Eng. Sci.*, **31**, 205 (1976).

Manuscript received Apr. 7, 1986, and revision received June 19, 1987.